Macromolecules
ARTICLE

Macromolecules **2010**, *43*, 9181–9190 **9181**
DOI: 10.1021/ma101860t

Chains Are More Flexible Under Tension

Andrey V. Dobrynin,*[†] Jan-Michael Y. Carrillo,[†] and Michael Rubinstein[‡]

[†]*Polymer Program, Institute of Materials Science and Department of Physics, University of Connecticut, Storrs, Connecticut 06269, United States, and* [‡]*Department of Chemistry, University of North Carolina, Chapel Hill, North Carolina 27599-3290, United States*

Received August 13, 2010; Revised Manuscript Received September 20, 2010

ABSTRACT: The mechanical response of networks, gels, and brush layers is a manifestation of the elastic properties of the individual macromolecules. Furthermore, the elastic response of macromolecules to an applied force is the foundation of the single-molecule force spectroscopy techniques. The two main classes of models describing chain elasticity include the worm-like and freely jointed chain models. The selection between these two classes of models is based on the assumptions about chain flexibility. In many experimental situations, the choice is not clear, and a model describing the crossover between these two limiting classes is therefore in high demand. We are proposing a unified chain deformation model that describes the force–deformation curve in terms of the chain bending constant, K, and bond length, b. This model demonstrates that the worm-like and freely jointed chain models correspond to two different regimes of polymer deformation, and the crossover between these two regimes depends on the chain bending rigidity and the magnitude of the applied force. Polymer chains with bending constant $K > 1$ behave as a worm-like chain under tension in the interval of the applied forces $f \leq Kk_BT/b$ and as a freely jointed chain for $f \geq Kk_BT/b$. (k_B is the Boltzmann constant and T is the absolute temperature.) The proposed crossover expression for chain deformation is in excellent agreement with the results of the molecular dynamics simulations of chain deformation and single-molecule deformation experiments of biological and synthetic macromolecules.

A polymer chain under tension is one of the classical problems of polymer physics.[1] The solution of this problem is of paramount importance for understanding swelling and deformation of polymeric and biological networks and gels[1−3] and deformation of polymer chains in external flow,[4] for elucidating factors controlling structure of polymer brushes,[5,6] and for analysis of force spectroscopy experiments.[7−9] The force spectroscopy experiments on DNA, RNA, actin, and microtubules filaments provide information about stresses and strains experienced by molecules during biological processes such as molecular recognition between DNA and proteins, protein-induced bending of DNA, cytoskeleton polymerization, and energy transduction during the ATP cycle in molecular motors.[7−9] Unfortunately, the interpretation of the force-elongation experiments and the obtained values of elastic constants is model-dependent and heavily relies on the assumptions used in the data analysis.

There are several models developed to describe chain deformation.[1] The freely jointed class of chain models[1] is usually applied to the deformations of flexible polymers. The deformations of stiff biological macromolecules such as DNA and biological filaments are described by the class of worm-like chains (WLCs).[9−11] In the small force limit, the models from both classes give a linear relationship between the magnitude of the applied force, f, and the chain elongation along the force direction, R_f,[1] but at large pulling forces, the models from these two classes demonstrate qualitatively different power law dependences of the tension f on the difference between the chain size R_f and its maximum value $R_{\max}$. For the models belonging to the class of freely jointed chains (FJCs), the force is inversely proportional to this difference, $f \propto (R_{\max} - R_f)^{-1}$, whereas for the models from the class of the WLCs, the force f exhibits a stronger divergence $f \propto (R_{\max} - R_f)^{-2}$.

Computer simulations of chain models with finite bending rigidity show the existence of two nonlinear deformation regimes under tension.[12−14] In the interval of the applied forces f smaller than the crossover value f_c, a polymer chain behaves as a WLC with force proportional to $f \propto (R_{\max} - R_f)^{-2}$. However, when the value of the applied force f exceeds the critical value f_c, one observes the FJC behavior $f \propto (R_{\max} - R_f)^{-1}$. The crossover between these two nonlinear deformation regimes is model-dependent and is controlled by the chain bending rigidity. The theoretical interpretation of these results was done on the scaling level by introducing force-dependent chain persistence length[14] or by using asymptotic results for strong chain deformations.[12,13] These approximations are reasonably good for very stiff chains for which the crossover between different nonlinear deformation regimes occurs in the limit of large chain deformations. However, for less stiff and more flexible chains, the crossover is located in the intermediate range of chain deformations, and the proposed approximations lead to large errors. Furthermore, the majority of experimental systems, for which crossover between different deformation regimes can be observed, belong to the class of flexible polymers. Therefore, accurate interpretation of the experimental results requires a more precise expression describing chain deformation in the entire interval of the applied forces.

In this Article, we study a discrete chain model with a bending potential. This model has a parameter, the effective bending constant; by changing which, one can crossover between WLC and FJC models. We present analytical solutions of this model that provide a crossover expression describing chain deformations in the entire interval of the applied forces with an accuracy better than 1%. We used this expression to describe the crossover between WLC and FJC models in terms of the chain rigidity and the magnitude of the applied force. Application of our expression to the results of single-molecule experiments and computer simulations suggests universality of the force-elongation dependence of polymer chains.

---

*To whom correspondence should be addressed.

Consider a chain with N bonds of constant length, b. The ends of this chain are pulled by a pair of external forces of equal magnitude f and opposite directions. For simplicity, we will assume that these external forces are parallel to the z axis. We can describe a chain conformation by a set of unit vectors $\vec{n}_i$ pointing along the chain bonds. The potential energy of the chain with the bending modulus k_BTK (where k_B is the Boltzmann constant, T is the absolute temperature, and K is the chain bending constant) in a given conformation includes contributions from the bending energy and from the external forces

$$\frac{U(\{\vec{n}_i\},\vec{f})}{k_BT} = \frac{K}{2}\sum_{i=0}^{N-2}(\vec{n}_i-\vec{n}_{i+1})^2-\sum_{i=0}^{N-1}\frac{b(\vec{f}\cdot\vec{n}_i)}{k_BT} \qquad (1)$$

The first term in the right-hand side of eq 1 describes the chain bending rigidity. The value of the parameter K controls the orientational correlations between bond vectors. In the case of the large values of the parameter $K \gg 1$, the potential energy of a polymer in our model (eq 1) describes a WLC under tension. However, as the value of the parameter K approaches zero, $K \to 0$, our model (eq 1) describes the deformation of a FJC. Therefore, by varying the value of the bending constant K, one can cover both WLC and FJC regimes.

We can evaluate chain deformation in the two limiting cases of small and large values of the applied forces. In the limit of weak forces, we can consider the force term in the rhs of eq 1 as a perturbation. Using this approximation, the average value of the projection of the unit bond vector on the force direction is equal to

$$\langle n_z\rangle = \langle N^{-1}\sum_{s=0}^{N-1} n_s^z\rangle \approx \frac{fb}{3k_BTN}\sum_{s,j=0}^{N-1}\langle(\vec{n}_s\cdot\vec{n}_j)\rangle_0$$

$$\approx \frac{fb_K}{3k_BT}, \quad \text{for} \quad fb_K \ll k_BT \qquad (2)$$

where brackets $\langle\ \rangle$ and $\langle\ \rangle_0$ denote averages with the statistical weights corresponding to the chain's potential energy $U(\{\vec{n}_i\},f)$ with and without force, respectively. (See eq 1.) This chain deformation regime is referred to as the linear deformation regime in the chain deformation diagram shown in reduced force $\tilde{f} = fb/k_BT$, bending constant K plane. (See Figure 1.)

The Kuhn length in our model is equal to

$$b_K = b\frac{1+\langle\cos(\theta)\rangle_0}{1-\langle\cos(\theta)\rangle_0} = b\frac{1+\coth(K)-K^{-1}}{1-\coth(K)+K^{-1}}$$

$$\approx \begin{cases} 2bK, & \text{for} \quad K \gg 1 \\ b, & \text{for} \quad K \ll 1 \end{cases} \qquad (3)$$

It depends on the average value $\langle\cos(\theta)\rangle_0$ of the cosine of the angle θ between two consecutive bond vectors along the polymer backbone. Note that in the case of large values of the bending parameter $K \gg 1$ the Kuhn length is equal to $b_K = 2bK$. In the opposite limit $K \ll 1$, the Kuhn length approaches the bond length, b. The average projection of the end-to-end vector on the direction of deformation is related to the average value of the projection of the unit bond vector on the direction of the applied force $\langle n_z\rangle$ by the equation

$$\langle R_z\rangle = Nb\langle n_z\rangle \qquad (4)$$

In the case of large magnitude of the applied force, $f > k_BT/b_K$, the average value of the projection of the unit vector on the direction of the applied force $\langle n_z\rangle$ is close to unity. In this regime, we can perform the mode spectrum analysis of the bond vectors $\vec{n}_i$. (See Appendix A.) This approach shows that the chain deformation and the magnitude of the applied force are related as follows

$$1-\langle n_z\rangle^2 \approx 2\langle n_z\rangle(\tilde{f}(4K\langle n_z\rangle+\tilde{f}))^{-1/2}, \quad \text{for} \quad b/b_K < \tilde{f} \qquad (5)$$

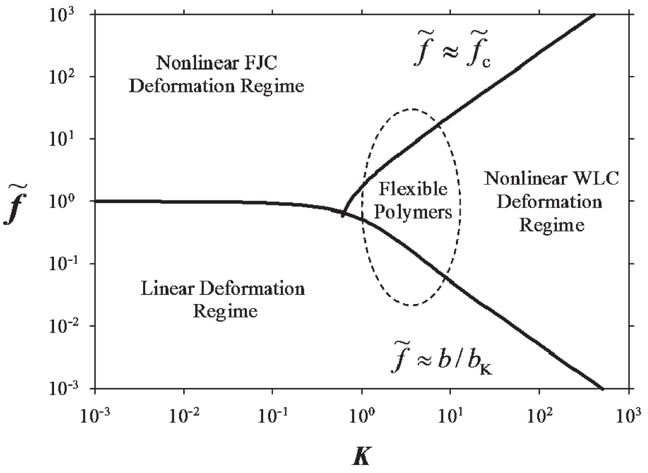

Figure 1. Diagram of different chain deformation regimes. $\tilde{f} = fb/k_BT$ is reduced force and K is bending constant. Solid lines are given by $\tilde{f} \approx \tilde{f}_c \approx 2.47K(1-0.5/K)^{1/2}$ and $\tilde{f} \approx b/b_K = (1-\coth K + K^{-1})/(1-\coth K - K^{-1})$. (See the text for details.) The ellipse shows the typical range of parameters corresponding to flexible polymers. Logarithmic scales.

Equation 5 can be transformed to the quadratic equation for the reduced force. The solution of this equation gives the relationship between the normalized external force $\tilde{f}$ and chain size $\langle R_z\rangle$ (or average projection of the bond unit vector $\langle n_z\rangle$, eq 4) in the nonlinear deformation regime.

$$\tilde{f} \approx 2\langle n_z\rangle K\left(\sqrt{1+\frac{1}{K^2(1-\langle n_z\rangle^2)^2}}-1\right), \quad \text{for} \quad b/b_K < \tilde{f} \qquad (6)$$

The interesting consequence of this equation is that there are two nonlinear regimes of the pulling force dependence on the average chain extension. In the intermediate force interval $b/b_K < \tilde{f} \ll K$ (or $K^{-1} \ll 1 - \langle n_z\rangle^2 \ll 1$), eq 6 reduces to

$$\tilde{f}K \approx \frac{\langle n_z\rangle}{(1-\langle n_z\rangle^2)^2} \approx \frac{1}{4(1-\langle n_z\rangle)^2},$$

$$\text{for} \quad b/b_K < \tilde{f} < K \qquad (7a)$$

This is exactly the expected dependence for the worm-like class of polymer chains under tension.[1] Note that the width of this regime shrinks with decreasing bending constant, K. (See the nonlinear WLC deformation regime in Figure 1.)

In the opposite limit of very large forces $\tilde{f} \gg K$ (or $1 - \langle n_z\rangle^2 \ll K^{-1} \ll 1$), we obtain

$$\tilde{f} \approx \frac{2\langle n_z\rangle}{1-\langle n_z\rangle^2} \approx \frac{1}{1-\langle n_z\rangle}, \quad \text{for} \quad \tilde{f} \gg K \qquad (7b)$$

Therefore, our model in the large force limit behaves as an FJC with polymer deformation being independent of the bending rigidity, K. (See the nonlinear FJC deformation regime in Figure 1.) This should not be surprising because in this limit the force term in eq 1 dominates over the bending term and controls chain elasticity on length scales smaller than the Kuhn length.

A more accurate location of the crossover between the nonlinear WLC and nonlinear FJC deformation regimes can be obtained by equating eqs 7a and 7b, solving the resultant equation for $\langle n_z\rangle \approx (1 - 1/(2K))^{1/2}$, and substituting this solution into eq 6. This results in the following equation describing the crossover line

$$\tilde{f}_{\mathrm{c}} \approx 2.47K(1-0.5/K)^{1/2} \qquad (8)$$

This equation is shown as a solid line separating nonlinear FJC deformation regime and nonlinear WLC deformation regime in Figure 1. Note that eq 6 describing the nonlinear chain deformation can be reduced to the expressions derived in ref 12 by setting $\langle n_z \rangle \approx 1$ and approximating $1 - \langle n_z \rangle^2$ by $2(1 - \langle n_z \rangle)$.

Combining the force-elongation relation (eq 6) for the nonlinear chain deformations ($1 - \langle n_z \rangle^2 \ll 1$) with eq 2 for the linear chain deformation regime ($\langle n_z \rangle^2 \ll 1$), we propose a crossover expression that describes polymer deformation in the entire interval of applied forces

$$\frac{f}{k_{\mathrm{B}}T} \approx \frac{3\langle n_z \rangle}{b_{\mathrm{K}}} + \frac{2\langle n_z \rangle}{b}\left(\sqrt{K^2 + (1-\langle n_z \rangle^2)^{-2}} - \sqrt{K^2+1}\right) \qquad (9)$$

where we have added terms $\langle n_z \rangle(3/b_{\mathrm{K}} + 2(K - (K^2 + 1)^{1/2}/b)$ linear in $\langle n_z \rangle$ to ensure the proper linear force−extension dependence. (See eq 2.) Equation 9 is the main result of this Article. Note that for the discrete chain model with bending potential (eq 1), the Kuhn length depends on the bond length, b, and the value of the bending constant, K. (See eq 3.) Therefore, there are only two independent parameters that describe chain deformation. The Kuhn length, b_{K}, determines the chain elastic response at small deformations and the crossover to the nonlinear regime ($f \approx k_{\mathrm{B}}T/b_{\mathrm{K}}$), whereas the bending constant, K, controls force-elongation dependence in the intermediate range of the applied forces and the crossover ($f \approx \tilde{f}_c k_{\mathrm{B}}T/b$) between nonlinear WLC deformation regime and nonlinear FJC deformation regime. (See Figure 1.) It is interesting to point out that in the limit of large K, for which $b_{\mathrm{K}} \approx 2Kb$, eq 9 reduces to the expression for the deformation of semiflexible chains derived in ref 15

$$\frac{fbK}{k_{\mathrm{B}}T} \approx \frac{\langle n_z \rangle}{2} + \frac{\langle n_z \rangle}{(1-\langle n_z \rangle^2)^2}, \quad \text{for} \quad \tilde{f} < \tilde{f}_c \qquad (10)$$

Below we test our model of chain deformation by analyzing the single-molecule force−extension data from computer simulations and experiments. (The details of this analysis are given in Appendices B and C, respectively.)

To test how well eq 9 describes chain deformation, we have performed simulations of the bead−spring chains consisting of $N_{\mathrm{m}} = 200$ monomers with different values of the bending constant K. The simulation details are provided in Appendix B. Figure 2 displays the results of the molecular dynamics simulations of these chains under tension. The lines correspond to eq 9 where the Kuhn lengths b_{K} were calculated from the value of the bending constant K using the theoretical expression for this model (eq 3) and the bond length b was obtained from simulations for each set of bond potential parameters. (See Appendix B.) The agreement between the analytical expression for the chain deformation (eq 9) and the simulation results is excellent. The deviation between the simulations and the theoretical curves is <1% throughout the entire interval of chain deformations. There is a slightly larger deviation (~3%) of the analytical expression from the simulation results for chains with $K > 25$ in the small force limit. For these chains, the Kuhn length $b_{\mathrm{K}} \approx 2bK$ approaches their contour length bN, and one has to keep all terms in the sum in the eq 2 to correctly account for the finite N effects.

We have also used simulation results to compare the accuracy of different chain deformation models. (See Appendix D.)[12,14] The analysis shows that our eq 9 is the most accurate expression describing chain deformation in the entire interval of the applied forces. For example, for chain with $K = 1$, the maximum deviation of eq 9 from the simulation results does not exceed 1%. At the same time, the expression by Rosa et al.[12] shows a deviation of 6% for $\langle n_z \rangle \approx 0.5$. Even larger error ~10−15% in the same chain deformation range is observed for the Toan and Thirumalai expression.[14] The difference between expressions drops to <1% when the chain deformation $\langle n_z \rangle$ exceeds 0.9. The detailed comparison between different chain deformation models can be found in Appendix D.

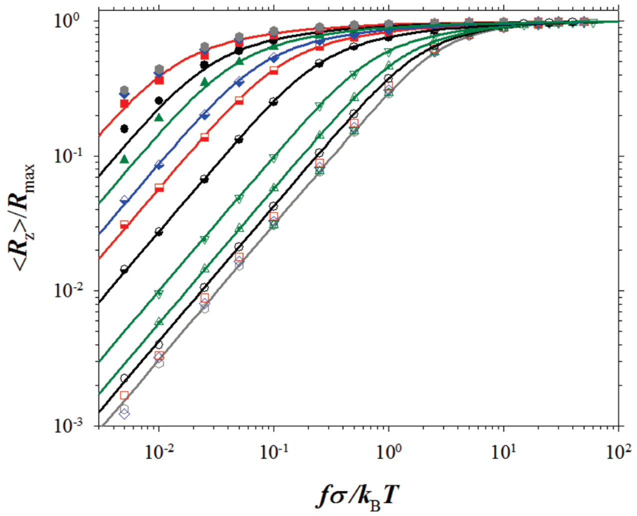

Figure 2. Deformation of discrete chains with number of monomers $N_{\mathrm{m}} = 200$ and with values of the bending constants: $K = 1/64$ (○), 1/32 (△), 1/16 (▽), 1/8 (◇), 1/4 (□), 1/2 (○), 1 (crossed triangles), 2 (inverted crossed triangles), 5 (⊖), 10 (⊟), 15 (half-filled rhombs), 25 (▲), 40 (●), 80 (■), 120 (◆), and 160 (⬢). The lines correspond to eq 9 with eq 3 used for calculation of b_K and with no adjustable parameters.

For the other models, such as freely rotating chain model,[1] the effective bending potential can only be defined for a sequence of several bonds. We need to define effective bonds of length b_{e} and effective bending constant K_{e} to map the force−elongation curves for this chain model onto our model (eq 1). For the discrete chain model, the value of the effective bond length b_{e} and the value of the effective bending constant K_{e} are related to each other by the equation analogous to eq 3

$$b_{\mathrm{e}} = b_{\mathrm{K}}\frac{1-\coth(K_{\mathrm{e}})+K_{\mathrm{e}}^{-1}}{1+\coth(K_{\mathrm{e}})-K_{\mathrm{e}}^{-1}} \qquad (11)$$

The Kuhn length b_{K} for the freely rotating chain model can be calculated from the analytical expression. (See eq B.5.)[1] In this case, we can substitute eq 11 for the effective bond length b_{e} into eq 9 and use eq 9 to evaluate the value of the bending constant K_{e} by fitting the chain deformation data to eq 9.

Figure 3 shows results of the molecular dynamics simulations of the freely rotating chain model. (See Appendix B for details.) The lines correspond to the best fit to eq 9 by considering K_{e} as an adjustable parameter. Inset shows the dependence of the effective chain bending constant on the value of the bond angle. Once again, we see an excellent agreement between simulation and analytical results. (See Appendix B for details.)

Similar analysis can be applied to describe deformation of other chain models[1] as well as experiments. To illustrate this, we have performed simulations of deformation of a chain with hindered internal rotations[1] and with the force-field parameters corresponding to polyethylene chain.[16] For this chain model, the force−elongation curve is close to that of a freely rotating chain with the value of the bond angle 50°. (See Figure 3.)

We applied eq 9 together with eq 11 to reanalyze the experimental data on single-chain deformation. In Figure 4, we plotted the dependence of the effective chain bending constant K_{e} on the

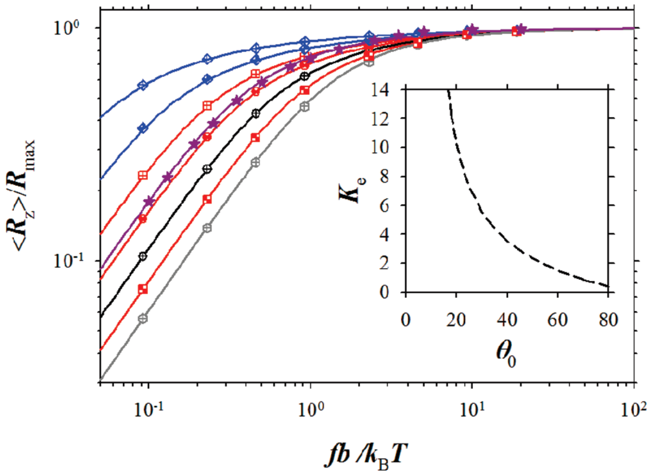

Figure 3. Deformation curves for freely rotating chains with the values of the bond angles $\theta_0 = 80$ (crossed gray hexagons), 70 (checkered red squares), 60 (⊕), 50 (red circles with hourglass), 40 (red ⊞), 30 (blue tilted squares with hourglass), and 20° (crossed blue rhombs) and for coarse-grained model of a PE chain (magenta ★). The lines correspond to the eq 9 by using K_e as an adjustable parameter. The values of the fitting parameters are given in Table B1. (See Appendix B.) The inset shows dependence of the effective bending constant K_e on the value of the bond angle.

ratio b_K/b_e of the Kuhn length to the effective bond length b_e for several different polymers including the single-stranded DNA at different salt concentrations,[17] polymethacrylic acid,[18] polystyrene,[19] polydimethylsiloxane,[20] dextran,[21] methlycellulose,[22] double-stranded DNA,[23] N2B domain of titin, and PEVK domain of titin.[24] (See Appendix C for details.) The data follow the line obtained for parameters of the discrete chain model with bending potential (eq 11), indicating a successful mapping of the real polymeric systems on our model.

To illustrate universality of the crossover between FJC and WLC for chains described by different chain models and for experiments, we combined simulation data for the discrete chain model with bending potential (eq 1), the freely rotating chain model, chain with hindered internal rotations, and experimental data and show in Figure 5 the dependence of the reduced force $\tilde f_e/\langle n_z\rangle K_e$ on the parameter $K_e(1-\langle n_z\rangle^2)$. The dashed line on this plot corresponds to eq 5, which describes both nonlinear deformation regimes as well as the crossover between them very well

$$\frac{\tilde f_e}{\langle n_z\rangle K_e} \approx 2\left(\sqrt{1+\frac{1}{K_e^2(1-\langle n_z\rangle^2)^2}}-1\right), \quad \text{for} \quad b_e/b_K < \tilde f_e \qquad (12)$$

Note that for the discrete chain model with bending potential (eq 1), $K_e = K$ and $b_e = b$. One can clearly identify two nonlinear chain deformation regimes in Figure 5. In the intermediate force interval $k_BT/b_K < f < K_e k_BT/b_e$, we observe the power law scaling $f \propto (1-\langle n_z\rangle^2)^{-2}$ representative of the WLC behavior, whereas in the large force limit, $K_e k_BT/b_e < f$, the scaling dependence changes to $f \propto (1-\langle n_z\rangle^2)^{-1}$. The surprising result of this plot is that even chains with bending constants $K = 1$ and 2, which one would consider to be flexible chains, still exhibit a WLC deformation dependence of the chain elongation on the applied force in the intermediate force range. The deviation from the universal curve at weak forces represents the crossover to the linear deformation regime with the average value of the projection of the unit bond vector on the direction of the applied force $\langle n_z\rangle$ proportional to the force f. (See Appendix A for details.) Note that the deviation from the universal behavior should also be observed in the limit of very large forces when chain elongation results in the deformation of the bond angles and bond lengths.[9,11]

The force f_c corresponding to the crossover between the WLC and FJC regimes depends on the value of the effective bending rigidity K_e and effective bond length b_e. Using eq 8, we can

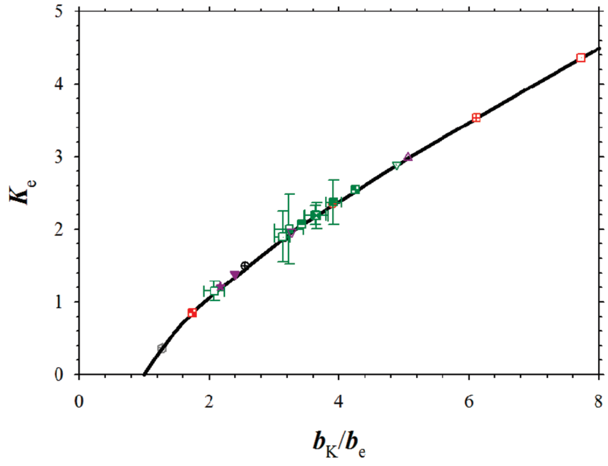

Figure 4. Dependence of the effective chain bending rigidity K_e on the ratio b_K/b_e of the Kuhn length to the effective bond length for a single-stranded DNA at different salt concentrations: 5 (green □), 4.0 (green ⊡), 3.0 (green ◨), and 2.0 M (green ◧); for PMMA (green squares, ⬓), polystyrene (green ⬒), PDMS (checker green square), dextran (hourglass green square), methylcellulose (magenta △), N2B domain of the protein titin (magenta ▽), and PEVK domain of the protein titin (magenta ▼); and simulation data for freely rotating chains with the values of the bond angles $\theta_0 = 80$ (crossed gray hexagons), 70 (checkered red squares), 60 (⊕), 50 (red circles with hourglass), 40 (red ⊞), and 35° (red square with a dot) and for coarse-grained model of a PE chain (magenta ★). The solid line corresponds to the discrete chain model with bending potential. (See eq 11.) The data points for this plot are summarized in Tables B1 and C1. (see Appendices B and C).

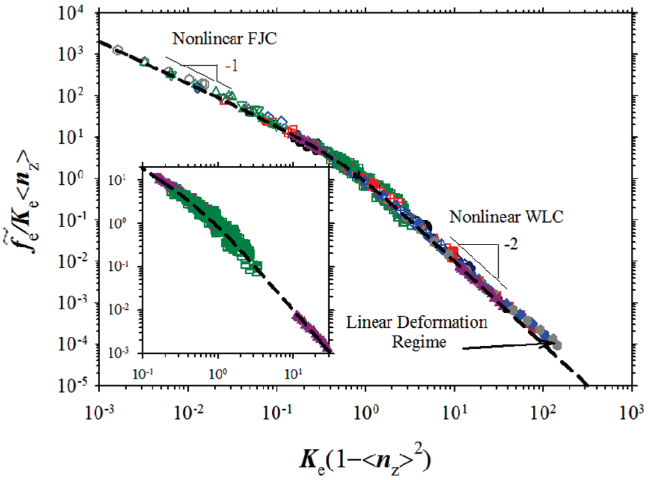

Figure 5. Universal plot describing deformations of semiflexible chains with bending constants $K = 1/64$ (gray ⬡), 1/32 (green △), 1/16 (green ▽), 1/8 (gray ◇), 1/4 (red □), 1/2 (black ○), 1 (crossed triangles), 2 (inverted crossed triangles), 5 (half filled circles), 10 (half filled squares), 15 (half filled rhombs), 25 (▲), 40 (●), 80 (■), 120 (◆), and 160 (⬢); freely rotating chains with 40 (crossed red squares) and 20° (crossed blue rhombs); for coarse-grained model of a PE chain (magenta ★). Experimental data for single-stranded DNA at different salt concentrations: 5 (green □), 4.0 (green ⊡), 3.0 (green ◨), and 2.0 M (green ◧); PMMA (green ⬓), polystyrene (green ⬒), PDMS (checker green square), dextran (hourglass green square), methylcellulose (magenta △), N2B domain of the protein titin (magenta ▽), PEVK domain of the protein titin (magenta ▼), and ddDNA (magenta ▲). The value of the reduced force for this plot was calculated as $\tilde f_e = fb_e/k_BT$. Inset shows only experimental data.

estimate the typical interval of forces where the crossover to the nonlinear FJC deformation regime can be observed for different experimental systems. For example, for flexible chains such as single-stranded DNA with a Kuhn length on the order of 1 to 1.5 nm, this crossover occurs between 10 and 100 pN, showing an increase with decreasing salt concentration. (See Appendix C, Table C1.) In the case of a rigid molecule such as double-stranded DNA with the persistence length on the order of 40 nm, the upper boundary of the WLC regime is located at $f \propto 4$ nN, which is outside the range of stability of double helix. Therefore, one can safely use the WLC model in the entire interval of the accessible forces for double-stranded DNA.

For simplicity, we did not take into account the interactions between the monomers that are remote along the polymer backbone. These interactions lead to chain swelling and can alter the chain behavior in the weak force limit.[1] However, we do not expect these effects to be significant in the case of nonlinear chain deformation and to change the crossover between WLC and FJC deformation regimes. The excluded volume interactions can only influence the location of the crossover to linear chain deformation regime. Note that our model can also be extended to include the effect of the bond elongation using the formalism developed in ref 15.

In conclusion, we have derived the crossover expression for chain deformation (eq 9), which correctly describes chain elongation in the entire interval of the applied forces. This expression confirms the existence of two nonlinear chain deformation regimes. With increasing force magnitude, the chain deformation first scales with the applied force as $\langle R_z \rangle / R_{\max} \propto 1 - (4 f K_e b_e / k_B T)^{-1/2}$ and then as $\langle R_z \rangle / R_{\max} \propto 1 - (f b_e / k_B T)^{-1}$. The force corresponding to the crossover between these two regimes is a function of the chain flexibility and is controlled by the effective bending rigidity, K_e, and the effective bond length, b_e. Our expression (eq 9) is in excellent agreement with the simulation results to an accuracy better than 1%. This expression for the force−deformation curve was used for the interpretation of the force spectroscopy data by considering b_K and K_e as fitting parameters. This allowed us to express parameters of the real polymeric systems in terms of the parameters describing deformation of the discrete chain model with bending potential. (See eq 1.)

The model of chain deformation presented in this paper can be applied to describe nonlinear elasticity of biological and polymeric networks and gels,[1−3,25] chain deformation in brush layers,[5] and structure of polyelectrolyte chains in dilute and semidilute solutions where electrostatic forces between ionized groups can result in strong chain elongation.[26] Our approach can also be extended to model deformation of molecular brushes and branched macromolecules.[27]

Acknowledgment. We are grateful to Prof. O. Saleh for providing the original data on ssDNA deformation. This work was supported by the National Science Foundation under the grant DMR-1004576, CHE-0911588, DMR-0907515, and CBET-0609087 and by the National Institutes of Health under grant 1-R01-HL077546-03A2.

Appendix A. Mode Spectrum Analysis of Chain Deformation

Below, we present details of the mode spectrum analysis of the chain's potential energy given by eq 1, extending the formalism developed in ref 15. To calculate averages with the Boltzmann weights corresponding to the chain's potential energy given by eq 1, it is useful to introduce the normal coordinates for a set of the bond vectors $\{\vec{n}_i\}$

$$\vec{\mathrm{n}}_s = \sum_{k=-(N-1)}^{N-1} \vec{\mathrm{a}}_k \exp\left(i \frac{\pi k s}{N}\right) \tag{A.1}$$

In this representation, the chain's potential energy is the quadratic function of the mode amplitudes

$$\frac{U(\{\vec{\mathrm{a}}_k\}, f)}{k_B T} = N \sum_{k=-(N-1)}^{N-1} \left(G(k) \frac{(\vec{\mathrm{a}}_k \cdot \vec{\mathrm{a}}_{-k})}{2} - \tilde{f} a_k^z t_k \right) \tag{A.2}$$

where we defined functions

$$G(k) = 2K(1 - \cos(k\pi/N)) \tag{A.3}$$

$$t_k = \frac{1}{N} \sum_{s=0}^{N-1} \exp\left(i \frac{\pi k s}{N}\right) \tag{A.4}$$

and used the expression for the reduced force $\tilde{f} = fb/k_B T$.

In the normal mode representation, the bond−bond correlation function $G(l)$ describing the decay of the orientational memory along the polymer backbone

$$G(l) = \frac{1}{N-l} \sum_{s=0}^{N-l-1} \langle (\vec{\mathrm{n}}_s \cdot \vec{\mathrm{n}}_{s+l}) \rangle \tag{A.5}$$

is equal to

$$G(l) = \sum_{k=-(N-1)}^{N-1} \langle (\vec{\mathrm{a}}_k \cdot \vec{\mathrm{a}}_{-k}) \rangle \exp\left(i \frac{k\pi l}{N}\right) \tag{A.6}$$

It is important to point out that the normal modes are not independent. This is due to the constraint on the value of the bond−bond correlation function $G(l)$ at $l = 0$, which should be equal to unity

$$1 = \sum_{k=-(N-1)}^{N-1} \langle (\vec{\mathrm{a}}_k \cdot \vec{\mathrm{a}}_{-k}) \rangle \tag{A.7}$$

To account for this constraint, we will introduce a Lagrange multiplier, μ, and modify the expression for the chain's potential energy as follows

$$\frac{U(\{\vec{\mathrm{a}}_k\}, f, \mu)}{k_B T} = N \sum_{k=-(N-1)}^{N-1} \left[(G(k) + \mu) \frac{(\vec{\mathrm{a}}_k \cdot \vec{\mathrm{a}}_{-k})}{2} - \tilde{f} t_k a_k^z \right] - \frac{N\mu}{2} \tag{A.8}$$

The complication in calculating averages with the chain's potential energy, given by eq A.8, arises because it requires knowledge of the orientations of the vector $\vec{a}_k$. Let us evaluate averages over mode amplitudes in two limiting cases of small and large values of the applied force. In the small force limit, $\tilde{f} \ll 1$, we can consider the force term in the rhs of the eq A.2 to be a perturbation. In this approximation, the average value of the projection of the unit bond vector on the direction of the force is equal to

$$\langle n_z \rangle = \langle N^{-1} \sum_{s=0}^{N-1} n_s^z \rangle = \sum_{k=-(N-1)}^{N-1} \langle a_k^z \rangle t_k$$

$$\approx N\tilde{f} \sum_{k=-(N-1)}^{N-1} \langle (a_k^z a_{-k}^z) \rangle_0 t_k t_{-k} \tag{A.9}$$

where brackets $\langle \ \rangle$ and $\langle \ \rangle_0$ denote averages with the statistical weights corresponding to $U(\{\vec{a}_k\}, f, \mu)$, and $U(\{\vec{a}_k\}, 0, \mu)$ respectively. To calculate the averages in eq A.9, we will set $\vec{a}_k = \vec{a}_{-k}$ and consider interval $k \geq 0$. This results in the following relations

$$\langle (a_0^z)^2 \rangle_0 = \frac{\langle \vec{\mathrm{a}}_0^{\,2} \rangle_0}{3} = \frac{2}{3\mu N} \tag{A.10}$$

$$\langle (a_k^z)^2 \rangle_0 = \frac{\langle \vec{\mathrm{a}}_k^{\,2} \rangle_0}{3} = \frac{(G(k) + \mu)^{-1}}{3N}$$

Note that in this approximation each vector $\vec{a}_k$ has only two independent components because eq A.1 is a linear transformation. Taking eq A.10 into account, the rhs of eq A.9 reduces to

$$\langle n_z\rangle \approx \frac{2\tilde{f}}{3\pi N}\sum_{s,s'=0}^{N-1}\int_0^{\pi}\frac{\mathrm{d}q\cos(q(s-s'))}{G(q)+\mu}$$

$$= \frac{\tilde{f}\langle R_0^2(\mu,K)\rangle}{3N},\quad \text{for}\quad \tilde{f}\ll 1 \tag{A.11}$$

where we defined

$$\langle R_0^2(\mu,K)\rangle = \frac{2}{\pi}\sum_{s,s'=0}^{N-1}\int_0^{\pi}\frac{\mathrm{d}q\cos(q(s-s'))}{G(q)+\mu} \tag{A.12}$$

In obtaining eq A.11, we have introduced $q = k\pi/N$ and substituted summation by integration.

In the case of large force amplitudes, we can assume that the average component of the vectors $\vec{a}_k$ points in the direction of the applied force. Therefore, the addition of the external constant force changes the average value of the amplitude of the mode component along the z axis to

$$\langle a_k^z\rangle \approx \tilde{f}t_{-k}/(G(k)+\mu),\quad \text{for}\quad \tilde{f}\gg 1 \tag{A.13}$$

resulting in the following expression for the average value of the unit bond vector

$$\langle n_z\rangle \approx \sum_{k=-(N-1)}^{N-1}\langle a_k^z\rangle t_k$$

$$\approx \frac{2\tilde{f}}{N\pi}\sum_{s,s'=0}^{N-1}\int_0^{\pi}\frac{\mathrm{d}q\cos((s-s')q)}{G(q)+\mu}-\frac{\tilde{f}}{\mu}$$

$$= \frac{\tilde{f}\langle R_0^2(\mu,K)\rangle}{N}-\frac{\tilde{f}}{\mu} \tag{A.14}$$

Combining eqs A.11 and A.14, we have

$$\langle n_z\rangle = \tilde{f}\begin{cases}\langle R_0^2(\mu,K)\rangle/3N, \tilde{f}\ll 1\\ \langle R_0^2(\mu,K)\rangle/N-1/\mu, \quad \tilde{f}\gg 1\end{cases} \tag{A.15}$$

where the Lagrange multiplier μ is the solution of the nonlinear equation

$$1 = \frac{2}{\pi}\int_0^{\pi}\frac{\mathrm{d}q}{G(q)+\mu}+\langle n_z\rangle^2 \tag{A.16}$$

Therefore, to obtain all averages, we have to know the integral in the following form

$$\frac{2}{\pi}\int_0^{\pi}\frac{\mathrm{d}q\cos(nq)}{2K+\mu-2K\cos(q)}$$

$$= \frac{2}{\pi(2K+\mu)}\int_0^{\pi}\frac{\mathrm{d}q\cos(nq)}{1-\beta\cos(q)}$$

$$= \frac{2}{(2K+\mu)\sqrt{1-\beta^2}}\left(\frac{1-\sqrt{1-\beta^2}}{\beta}\right)^n$$

$$= \frac{2}{\sqrt{\mu(4K+\mu)}}\left(\frac{1-\sqrt{1-\beta^2}}{\beta}\right)^n \tag{A.17}$$

where $\beta = 2K/(2K+\mu)$. (For evaluation of the integral, see G.R. 3.613.1.[28]) We can use eq A.17 to obtain the explicit expression for A.16

$$1-\langle n_z\rangle^2 = \frac{2}{\sqrt{\mu(4K+\mu)}} \tag{A.18}$$

and evaluate the value of

$$\langle R_0^2(\mu,K)\rangle \approx \frac{2N}{\sqrt{\mu(\mu+4K)}}\frac{1+B}{1-B} \tag{A.19}$$

where we have introduced

$$B = \beta^{-1}-\sqrt{\beta^{-2}-1} = 1+\frac{\mu}{2K}-\sqrt{\left(1+\frac{\mu}{2K}\right)^2-1}$$

$$= 1+\frac{\mu}{2K}-\sqrt{\frac{\mu}{2K}\left(2+\frac{\mu}{2K}\right)} \tag{A.20}$$

Consider two limiting cases

$$B \approx \begin{cases}1-\sqrt{\mu/K}, & \mu < 2K\\ K/\mu, & \mu > 2K\end{cases} \tag{A.21}$$

Substitution of these solutions into eq A.19 shows that the value of the Lagrange multiplier, controlling the norm of the unit bond vector, is equal to

$$\mu \approx \frac{\tilde{f}}{\langle n_z\rangle} \tag{A.22}$$

in the large force limit. This reduces eq A.18 to

$$1-\langle n_z\rangle^2 \approx \frac{2\langle n_z\rangle}{\sqrt{\tilde{f}(4K\langle n_z\rangle+\tilde{f})}} \tag{A.23}$$

The force−deformation relation covering the entire interval of the applied force can be described by the following crossover equation

$$\frac{f}{k_{\mathrm{B}}T} \approx \frac{3\langle n_z\rangle}{b_{\mathrm{K}}}+\frac{2\langle n_z\rangle}{b}\left(\sqrt{K^2+(1-\langle n_z\rangle^2)^{-2}}-\sqrt{K^2+1}\right) \tag{A.24}$$

To illustrate different regimes of chain deformation, we plot dependence of the reduced force $\tilde{f}/K\langle n_z\rangle$ on the chain deformation parameter $K(1-\langle n_z\rangle^2)$ in Figure A1. One can clearly identify three different regimes of chain deformation: the FJC regime in the large force interval, the WLC regime in the intermediate force interval, and linear deformation regime where the average value of the projection of the unit vector on the direction of the applied force is proportional to the force magnitude, $\langle n_z\rangle \propto \tilde{f}$. The lines end at points with coordinates $(K, 3b/Kb_{\mathrm{K}})$. The crossover to the linear chain deformation regime is manifested by the deviation of the chain deformation curves from the universal line with slope -2, describing the chain's deformation in the nonlinear WLC regime.

Appendix B. Simulation Details

Chains with Bending Potential. We performed simulations of different chain models under tension. First, we will outline simulation details for the discrete chain model with bending potential. A chain was modeled by a bead−spring chain consisting of $N_{\mathrm{m}} = 200$ monomers with diameter σ. The

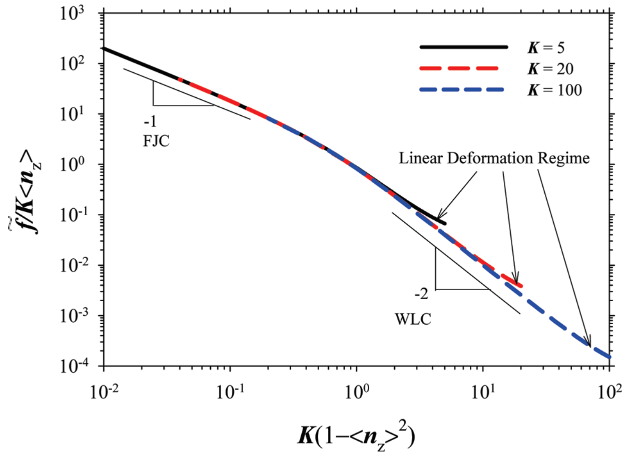

Figure A1. Universal plot describing deformations of the discrete chain model with bending potential for different values of bending constants.

monomers were connected to a chain by the finite extension nonlinear elastic (FENE) potential[29]

$$U_{\mathrm{FENE}}(r) = -0.5k_{\mathrm{spring}}R_{\max}^2 \ln\left(1-\frac{r^2}{R_{\max}^2}\right) \tag{B.1}$$

where k_{spring} is the spring constant and the maximum bond length is $R_{\max} = 1.5\sigma$. The repulsive part of the bond potential was modeled by the truncated shifted Lennard-Jones potential. We have performed simulations of chains with $k_{\mathrm{spring}} = 100k_BT/\sigma^2$, $\varepsilon_{\mathrm{LJ}} = 1.0k_BT$, $K = 1, 2$, and 5 and $k_{\mathrm{spring}} = 30k_BT/\sigma^2$, $\varepsilon_{\mathrm{LJ}} = 0.34k_BT$ for all other values of the chain bending constants K. The larger value of the spring constant was selected to minimize the effect of the bond stretching at large chain deformations. In our simulations, the values of the bond length were equal to $b = 0.9032\sigma$ and 0.9175σ for strong and weak spring constants, respectively. In the case of the weak bonds, the bond length increases to 0.948 (5% increase) for $f\sigma/k_BT = 20$, whereas for the strong bonds, it is equal to 0.918 (0.5% increase).

The chain bending rigidity was introduced to the model through a bending potential controlling the mutual orientations between two neighboring along the polymer backbone unit bond vectors $\vec{n}_i$ and $\vec{n}_{i+1}$

$$U_{i,i+1}^{\mathrm{bend}} = k_BTK(1-(\vec{\mathrm{n}}_i\cdot\vec{\mathrm{n}}_{i+1})) \tag{B.2}$$

The bending constant K was varied between 1/64 and 160.

The simulations were performed at a constant temperature, which was maintained by coupling the system to the Langevin thermostat. The motion of monomers was described by the following equations,

$$m\frac{\mathrm{d}\vec{\mathrm{v}}_i(t)}{\mathrm{d}t} = \vec{\mathrm{F}}_i(t) - \xi\vec{\mathrm{v}}_i(t) + \vec{\mathrm{F}}_i^R(t) \tag{B.3}$$

where m is the bead mass, $\vec{v}_i(t)$ is the bead velocity, and $\vec{F}_i(t)$ denotes the net deterministic force acting on the ith bead. The stochastic force $\vec{F}_i^R(t)$ has a zero-average value $\langle\vec{F}_i^R(t)\rangle = 0$ and δ-functional correlations $\langle\vec{F}_i^R(t)\vec{F}_i^R(t')\rangle = 6k_BT\xi\delta(t-t')$.[29] The friction coefficient ξ was set to $\xi = 0.143m/\tau_{\mathrm{LJ}}$, where τ_{LJ} is the standard LJ time $\tau_{\mathrm{LJ}} = \sigma(m/k_BT)^{1/2}$. The velocity–Verlet algorithm with a time step $\Delta t = 0.01\tau_{\mathrm{LJ}}$ was used for integration of the equations of motion eq B.3. We performed simulations by using the following procedure: at the beginning of each simulation run, a chain in a random walk configuration was placed in the center of the simulation box. A pair of constant forces, f, was applied to both ends of a chain pointing in opposite directions along the z axis. The magnitude of the force was varied between 10^{-3} and $50\,k_BT/\sigma$. The system was pre-equilibrated for 2×10^7 MD steps. This was followed by a production run lasting 2×10^8 MD steps. All simulations were performed using LAMMPS.[29]

Freely-Rotating Chain Model. In addition to simulations of the discrete chain model with bending potential, we performed simulations of chains described by the freely-rotating chain model with values of the bond angles θ_0 between 80 and 15°. The values of the bond angles were fixed by imposing a parabolic bond angle potential

$$U_{\mathrm{angle}}(\theta) = K_{\mathrm{angle}}(\theta-\theta_0)^2 \tag{B.4}$$

where $K_{\mathrm{angle}} = 300k_BT/\mathrm{rad}^2$. The bond length in these simulations was maintained by the FENE and truncated shifted Lennard-Jones potentials with $k_{\mathrm{spring}} = 30k_BT/\sigma^2$ and $\varepsilon_{\mathrm{LJ}} = 0.34k_BT$. The Kuhn length for this model is equal to[1]

$$b_K = \frac{b}{\cos(\theta_0/2)}\frac{1+\cos(\theta_0)}{1-\cos(\theta_0)} \tag{B.5}$$

Chain Model with Hindered Rotations. To compare the different models of polymer chains with the models of real chains, we performed molecular dynamics simulations of the deformation of chains with dihedral potential corresponding to a coarse-grained model of a polyethylene chain. The bond, bond angle, and dihedral angle potentials for this chain model are

$$U = K_{\mathrm{bond}}(r-r_0)^2 + K_{\mathrm{angle}}(\theta-\theta_0)^2 + A + B\cos(\phi) + C\cos^3(\phi) \tag{B.6}$$

where $r_0 = 1.526$ Å, $K_{\mathrm{bond}} = 260$ kcal/mol Å^2, $\theta_0 = 67.6°$, $K_{\mathrm{angle}} = 63$ kcal/mol rad^2, $A = 2$ kcal/mol, $B = -4.4$ kcal/mol, and $C = 6.4$ kcal/mol. The force field parameters for bond and bond angle are from the AMBER force field,[30] and the dihedral potential parameters are from Sumpter et al.[16] The simulations were performed at temperature $T = 300$ K. The chain degree of polymerization for these simulations was $N_m = 200$. The integration time step was 1.0 fs, and simulations continued for 200 ns. The value of the Kuhn length for this model is equal to[1]

$$b_K = \frac{b}{\cos(\theta_0/2)}\frac{1+\cos(\theta_0)}{1-\cos(\theta_0)}\frac{1+\langle\cos(\phi)\rangle}{1-\langle\cos(\phi)\rangle} \tag{B.7}$$

In Table B1, we summarized the fitting parameters for force–elongation curves obtained from MD simulations of freely rotating and PE chain models. The quality of the fit is characterized by the value of fit uncertainty σ_n. (See eq D.6.)

Appendix C. Comparison with Experiments

We applied eq 9 to analyze the force–chain deformation curves for single-stranded DNA in salt solutions of different ionic strengths,[17] polymethacrylic acid,[18] polystyrene,[19] polydimethylsiloxane,[20] dextran,[21] methlycellulose,[22] double-stranded DNA,[23] N2B domain of titin, and PEVK domain of titin.[24] In experiments, one usually measures the average projection of the end-to-end distance $\langle R_z\rangle$ on the direction of the applied force as a function of the force magnitude. Unfortunately, the exact value of the chain degree of polymerization is unknown. Therefore, we have modified our eq 8 and considered the size of the fully

Table B1

	b_K	b_e	K_e	σ_n	legend
freely rotating chain, $\theta_0 = 80°$	1.701σ	1.334σ	0.366	6.3×10^{-3}	gray hexagon, crossed
freely rotating chain, $\theta_0 = 70°$	2.283σ	1.309σ	0.851	6.0×10^{-3}	red square, checker
freely rotating chain, $\theta_0 = 60°$	3.173σ	1.245σ	1.493	4.6×10^{-3}	black circle, crossed
freely rotating chain, $\theta_0 = 55°$	3.809σ	1.211σ	1.890	3.5×10^{-3}	black circle with a dot
freely rotating chain, $\theta_0 = 50°$	4.641σ	1.188σ	2.347	2.5×10^{-3}	red circle, hourglass
freely rotating chain, $\theta_0 = 45°$	5.764σ	1.181σ	2.887	2.2×10^{-3}	inverted green triangle with a dot
freely rotating chain, $\theta_0 = 40°$	7.329σ	1.200σ	3.533	3.0×10^{-3}	red square, crossed
freely rotating chain, $\theta_0 = 35°$	9.602σ	1.243σ	4.357	3.9×10^{-3}	red square with a dot
freely rotating chain, $\theta_0 = 30°$	13.084σ	1.313σ	5.483	4.2×10^{-3}	blue rhombs, hourglass
freely rotating chain, $\theta_0 = 25°$	18.806σ	1.406σ	7.187	3.4×10^{-3}	blue rhombs with a dot
freely rotating chain, $\theta_0 = 20°$	29.181σ	1.528σ	10.051	1.6×10^{-3}	blue rhombs, crossed
freely rotating chain, $\theta_0 = 15°$	50.880σ	1.668σ	15.748	2.3×10^{-3}	blue rhombs, semifilled right
hindered rotation model of polyethylene	0.854 nm	0.393 nm	1.212	1.3×10^{-2}	magenta stars

Table C1

	b_K (nm)	b_e (nm)	K_e	f_{b_K}(pN)	f_c (pN)	legend
single-stranded DNA, 5.0 M NaCl buffer[17]	1.15 ± 0.10	0.55 ± 0.07	1.15 ± 0.13	3.58	15.97	green open square
single-stranded DNA, 4.0 M NaCl buffer[17]	1.11 ± 0.09	0.36 ± 0.04	1.90 ± 0.35	3.71	46.04	green square with a dot
single-stranded DNA, 3.0 M NaCl buffer[17]	1.27 ± 0.06	0.35 ± 0.02	2.19 ± 0.13	3.24	55.86	green square, semifilled right
single-stranded DNA, 2.0 M NaCl buffer[17]	1.33 ± 0.08	0.34 ± 0.04	2.37 ± 0.31	3.09	62.92	green square, semifilled left
polymethacrylic acid (PMAA)[18]	0.40 ± 0.04	0.12 ± 0.02	2.00 ± 0.48	10.29	146.68	green square, semifilled bottom
polystyrene[19]	0.65	0.19	2.06	6.33	95.88	green square, semifilled top
polydimethylsiloxane (PDMS)[20]	0.43	0.10	2.54	9.89	239.09	green square, checker
dextran[21]	0.72 ± 0.11	0.20 ± 0.02	2.19 ± 0.18	5.71	97.75	green square, hourglass
methlycellulose[22]	0.48	0.10	2.98	8.51	276.27	magenta open triangle
double-stranded DNA, 20 mM Tris, 130 mM K^+, 4 mM Mg^{2+} (PTC buffer, pH 8.0)[23]	82.93	0.34	121.96	0.05	3637.84	magenta filled triangle
N2B domain of titin[24]	0.78	0.24	1.97	5.31	72.54	magenta open inverted triangle
PEVK domain of titin[24]	1.40	0.44	1.34	2.95	24.52	magenta filled inverted triangle

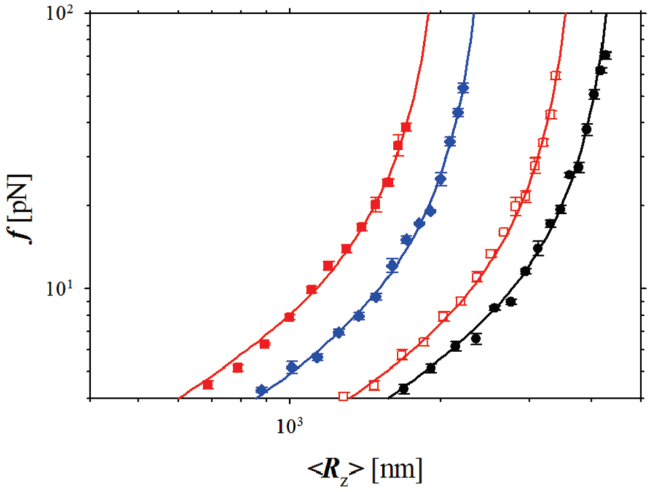

Figure C1. Dependence of the magnitude of the applied force f on the chain length $\langle R_z \rangle$ for single-stranded DNA molecules of four different lengths at salt concentration 5 M. The lines are the best fit to eq C.1.

extended chain R_{max} as an additional adjustable parameter. With this modification, eq 9 transforms to

$$\frac{f}{k_B T} \approx \frac{3\langle R_z \rangle}{b_K R_{max}} + \frac{2\langle R_z \rangle}{b_e R_{max}} \left(\sqrt{K_e^2 + (1 - (\langle R_z \rangle / R_{max})^2)^{-2}} - \sqrt{K_e^2 + 1} \right) \tag{C.1}$$

where we substituted $\langle n_z \rangle = \langle R_z \rangle / R_{max}$. The value of the effective bond length b_e for the fitting procedure was set to

$$b_e = b_K \frac{1 - \coth(K_e) + K_e^{-1}}{1 + \coth(K_e) - K_e^{-1}} \tag{C.2}$$

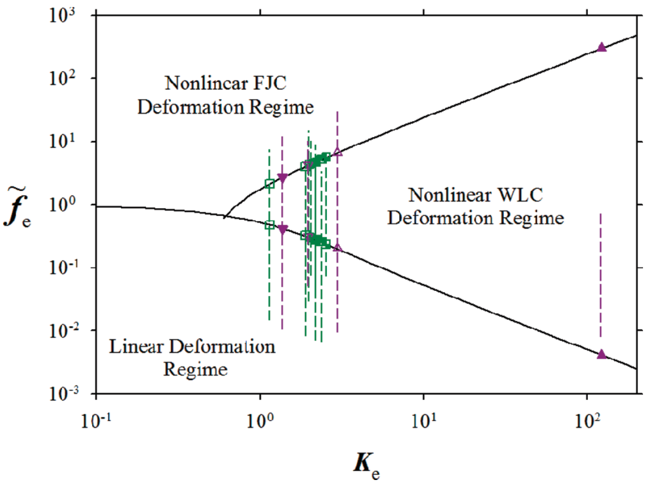

Figure C2. Diagram of different chain deformation regimes. $\tilde{f}_e = f b_e / k_B T$ is the reduced force. Solid lines represent crossover between different chain deformation regimes and are given by the eqs 3 and 8. Dashed lines show the intervals of forces covered in experiments. Logarithmic scales.

In Figure C1, we show the results of the least-squares fitting procedure of the deformation curves of the single-stranded DNA molecules of four different lengths stretched at salt concentration 5 M[17] to our eq C.1 by considering R_{max}, b_K, and K_e as adjustable parameters. The agreement between eq C.1 and the experimental data is very good. The values of the fitting parameters and of the effective bond length b_e are summarized in Table C1. Note that the same procedure was used to fit experimental data for all other polymeric systems. For fitting double-stranded DNA data, we set $b_e = 0.34$ nm, which corresponds to the average projection length per base pair.

Using values of the fitting parameters given in Table C1, one can obtain values of the forces that separate different chain deformation regimes shown in Figure 1. In Figure C2, we replotted Figure 1 and added the data points corresponding to the values of the crossover forces obtained from the fitting parameters of the chain deformation curves. The dashed lines in Figure C2 correspond to experimentally accessible force intervals before energetic effects due to bond length and bond angle deformations start to contribute to the chain elasticity.

Appendix D. Comparison of Different Expressions for Chain Deformation

In this section, we will establish the accuracy of the different expressions[12,14] for chain deformations by comparing the expressions with the simulation results for the discrete chain model with bending potential. Below we will compare our expression eq 9

$$\frac{f_{\mathrm{DCR}}}{k_{\mathrm{B}}T} \approx \frac{3\langle n_z\rangle}{b_{\mathrm{K}}} + \frac{2\langle n_z\rangle}{b}\left(\sqrt{K^2+(1-\langle n_z\rangle^2)^{-2}} - \sqrt{K^2+1}\right) \quad (\mathrm{D.1})$$

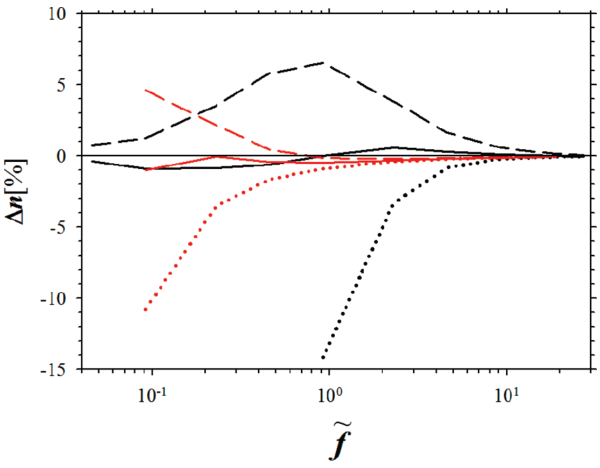

Figure D1. Dependence of deviation parameter Δn, given by eq D.4 on the reduced force $\tilde{f} = fb/k_{\mathrm{B}}T$. The lines show normalized difference Δn between simulation data and eqs D.1 (—), D.2 (– – –), D.3 (···) for different values of the chain bending constant $K = 1$ (black) and 10 (red).

with expressions derived by Rosa et al.[12]

$$\frac{f_{\mathrm{R}}}{k_{\mathrm{B}}T} \approx \left(\frac{3}{b_K} - \frac{1}{b\sqrt{4K^2+1}}\right)\langle n_z\rangle + \frac{1}{b}\left(\sqrt{4K^2+(1-\langle n_z\rangle)^{-2}} - \sqrt{4K^2+1}\right) \quad (\mathrm{D.2})$$

and by Toan and Thirumalai[14]

$$\frac{f_{\mathrm{TT}}}{k_{\mathrm{B}}T} \approx \frac{1}{b}\left(\sqrt{4K^2+(1-\langle n_z\rangle)^{-2}} - 2K\right) \quad (\mathrm{D.3})$$

which we have rewritten in terms of the parameters of our model and set the exponent $\alpha = 2$ in the Toan and Thirumalai expression.[14] It follows from eq D.2 that the Toan and Thirumalai expression[14] corresponds to a large force deformation limit of the Rosa et al. expression.[12] In Figure D1, we present the normalized difference between the average value of the projection of the unit bond vector on the force direction obtained from molecular dynamics simulations of the discrete chain model with bending potential and those obtained from eqs D.1−D.3

$$\Delta n = 1 - \frac{\langle n_z^{\mathrm{th}}(\tilde{f})\rangle}{\langle n_z^{\mathrm{sim}}(\tilde{f})\rangle} \quad (\mathrm{D.4})$$

It follows from this Figure that our expression is the closest to the simulation results with accuracy better than 1% throughout significant interval of the applied forces. Note that in our comparison of the simulation results with the Toan and Thirumalai expression[14] eq D.3, we only used the interval of the applied forces for which $\langle n_z\rangle > 0.5$. This interval of chain deformations was used by Toan and Thirumalai to fit the experimental data. All expressions show a very good agreement with the simulation results in the case of strong chain deformations. It should not be surprising because all three expressions converge to the same asymptotic expression in the limit $\langle n_z\rangle \to 1$. However, eqs D.2 and D.3 show larger deviations from simulation results in the range of intermediate forces.

Let us now solve an inverse problem by considering simulation data as deformation data of a chain with unknown value of the bending rigidity, K. By performing this test, we will establish how accurate different expressions for chain deformation can recover

Table D1

Inverse Problem for Discrete Chain Model with Bending Rigidity

K_{sim}	K		error (%)		σ_n	
	D.1	*D.2*	*D.1*	*D.2*	*D.1*	*D.2*
1.0	0.999	1.117	0.1	11.7	1.6×10^{-3}	6.1×10^{-3}
10.0	9.750	10.261	2.5	2.6	2.1×10^{-3}	5.7×10^{-3}

Freely Rotating Chain Model and Coarse Grained Polyethylene Chain

	K_{e}		σ_n	
	D.1	*D.2*	*D.1*	*D.2*
freely rotating chain, $\theta_0 = 70°$	0.851	0.692	6.0×10^{-3}	1.4×10^{-2}
freely rotating chain, $\theta_0 = 50°$	2.347	2.147	2.4×10^{-3}	1.4×10^{-2}
freely rotating chain, $\theta_0 = 20°$	10.051	9.534	1.6×10^{-3}	9.8×10^{-3}
hindered rotation model of polyethylene	1.212	0.895	1.3×10^{-2}	1.4×10^{-2}

Single-Stranded DNA at 5.0 M NaCl Buffer

	b_{K} (nm)		b_{e} (nm)		K_{e}		$R_{\max}$ (nm)		σ_n	
	D.1	*D.2*	*D.1*	*D.2*	*D.1*	*D.2*	*D.1*	*D.2*	*D.1*	*D.2*
1	1.20	1.35	0.66	0.79	0.92	0.82	4518.32	4470.59	1.6×10^{-2}	1.7×10^{-2}
2	0.98	1.1	0.45	0.52	1.22	1.18	2048.79	2032.65	1.3×10^{-2}	1.2×10^{-2}
3	1.22	1.35	0.55	0.73	1.23	0.94	3748.83	3721.01	1.6×10^{-2}	1.7×10^{-2}
4	1.20	1.34	0.55	0.61	1.22	1.25	2492.00	2478.82	1.1×10^{-2}	1.3×10^{-2}
ave	1.15	1.29	0.55	0.66	1.15	1.05				

the value of the chain bending constant. We performed this test for chains with $K = 1$ and 10. The simulation data were fitted by using the least-squares fitting procedure by minimizing the difference

$$\chi(K) = \sum_{p=1}^{N_p} (1 - \tilde{f}^{\mathrm{th}}(\langle n_z \rangle_p)/\tilde{f}_p^{\mathrm{sim}})^2 \qquad \text{(D.5)}$$

with respect to chain bending rigidity, K. Summation in eq D.5 is performed over all simulation points N_p. The ratio of b_K/b for this chain model is given by eq 3. The accuracy of the fitting procedure was evaluated by calculating the uncertainty

$$\sigma_n = \sqrt{\frac{1}{N_\mathrm{p}} \sum_{p=1}^{N_\mathrm{p}} (\langle n_z \rangle_p^{\mathrm{sim}} - \langle n_z \rangle_p^{\mathrm{th}})^2} \qquad \text{(D.6)}$$

The results of this test are listed in Table D1. It follows from this Table that our eq D.1 performs better than eq D.2 for both sets of simulation data. The largest difference between the actual value of the chain bending constant K and the one obtained from the fitting procedure is observed for eq D.2 and data set corresponding to $K = 1$. The fitting method of the simulation data to eq D.2 gives the value of the parameter K equal to $K = 1.12$ with the error of 12% (to be compared with 0.1% error for fitting this data set $K = 1$ by eq D.1). The agreement between actual value of the bending constant and ones obtained from the fitting procedure improves with increasing the chain bending rigidity.

Similar tests were conducted for the freely rotating chain model and the coarse-grained model of a polyethylene chain. Both expressions produced comparable values of the chain bending constants. However, our expression eq D.1 shows smaller value of the uncertainty σ_n. (See Table D1.)

In the case of the analysis of the experimental data, the number of the fitting parameters increases to three because in addition to Kuhn length, b_K, and bending constant, K_e, one has to simultaneously optimize the maximum chain length, R_max. (See Appendix C.) In this case, fitting by both eqs D.1 and D.2 provides close value of the maximum chain length R_max. (See Table D1.) There is a larger difference in the values of the chain bending constant K_e and Kuhn length b_K. The values of uncertainty are close for both fits. This shows that the advantage of a more accurate expression diminishes with increasing the number of the adjustable parameters and the decreasing accuracy of data.

References and Notes

(1) Rubinstein, M.; Colby, R. H. *Polymer Physics*; Oxford University Press: New York, 2003.

(2) Treloar, L. R. G. *The Physics of Rubber Elasticity*; Clarendon Press: Oxford, New York, 2005.

(3) Janmey, P. A.; McCormick, M. E.; Rammensee, S.; Leight, J. L.; Georges, P. C.; MacKintosh, F. C. Negative normal stress in semiflexible biopolymer gels. *Nat. Mater.* **2007**, *6*, 48–51.

(4) Larson, R. G. The rheology of dilute solutions of flexible polymers: progress and problems. *J. Rheol.* **2005**, *49*, 1–70.

(5) Minko, S. Responsive polymer brushes. *Polym. Rev.* **2006**, *46*, 397–420.

(6) Rühe, J.; Ballauff, M.; Biesalski, M.; Dziezok, P.; Gröhn, F.; Johannsmann, D.; Houbenov, N.; Hugenberg, N.; Konradi, R.; Minko, S.; Motornov, M.; Netz, R. R.; Schmidt, M.; Seidel, C.; Stamm, M.; Stephan, T.; Usov, D.; Zhang, H. Polyelectrolyte brushes. *Adv. Polym. Sci.* **2004**, *165*, 79–150.

(7) Neuman, K. C.; Lionnet, T.; Allemand, J. F. Single-molecule micromanipulation techniques. *Annu. Rev. Mater. Res.* **2007**, *37*, 33–67.

(8) Neuman, K. C.; Nagy, A. Single-molecule force spectroscopy: optical tweezers, magnetic tweezers and atomic force microscopy. *Nat. Methods* **2008**, *5*, 491–505.

(9) Williams, M. C.; Rouzina, I. Force spectroscopy of single DNA and RNA molecules. *Curr. Opin. Struct. Biol.* **2002**, *12*, 330–336.

(10) Marko, J. F.; Siggia, E. D. Stretching DNA. *Macromolecules* **1995**, *28*, 8759–8770.

(11) Bustamante, C.; Smith, S. B.; Liphardt, J.; Smith, D. Single-molecule studies of DNA mechanics. *Curr. Opin. Struct. Biol.* **2000**, *10*, 279–285.

(12) Rosa, A.; Hoang, T. X.; Marenduzzo, D.; Maritan, A. Elasticity of semiflexible polymers with and without self-interactions. *Macromolecules* **2003**, *36*, 10095–10102.

(13) Livadaru, L.; Netz, R. R.; Kreuzer, H. J. Stretching response of discrete semiflexible polymers. *Macromolecules* **2003**, *36*, 3732–3744.

(14) Toan, N. M.; Thirumalai, D. Theory of biopolymer stretching at high force. *Macromolecules* **2010**, *43*, 4394–4400.

(15) Carrillo, J.-M. Y.; Dobrynin, A. V. Effect of the electrostatic interactions on stretching of semiflexible and biological polyelectrolytes. *Macromolecules* **2010**, *43*, 2589–2604.

(16) Sumpter, B. G.; Noid, D. W.; Wunderlich, B. Computational experiments on the motion and generation of defects in polymer crystals. *Macromolecules* **1992**, *25*, 7247–7255.

(17) Saleh, O. A.; McIntosh, D. B.; Pincus, P.; Ribeck, N. Nonlinear low-force elasticity of single-stranded DNA molecules. *Phys. Rev. Lett.* **2009**, *102*, 068301-1–068301-4.

(18) Ortiz, C.; Hadziioannou, G. Entropic elasticity of single polymer chains of poly(methacrylic acid) measured by atomic force microscopy. *Macromolecules* **1999**, *32*, 780–787.

(19) Nakajima, K.; Watanabe, H.; Nishi, T. Single polymer chain rubber elasticity investigated by atomic force microscopy. *Polymer* **2006**, *47*, 2505–2510.

(20) Senden, T. J.; Meglio, J.-M.; Auroy, P. Anomalous adhesion in adsorbed polymer layers. *Eur. Phys. J. B* **1998**, *3*, 211–216.

(21) Reif, M.; Oesterhelt, F.; Heymann, B.; Gaub, H. E. Single molecule force spectroscopy on polysaccharides by atomic force microscopy. *Science* **1997**, *275*, 1295–1297.

(22) Lee, G.; Nowak, W.; Jaroniec, J.; Zhang, Q.; Marszalek, P. E. Molecular dynamics simulations of force conformational transition in 1,6-linked polysaccharides. *Biophys. J.* **2004**, *87*, 1456–1465.

(23) Wang, M. D.; Yin, H.; Landick, R.; Gelles, J.; Block, S. M. Stretching DNA with optical tweezers. *Biophys. J.* **1997**, *72*, 1335–1346.

(24) Li, H.; Linke, W. A.; Oberhauser, A. F.; Carrion-Vazquez, M.; Kerkvliet, J. G.; Lu, H.; Marszalek, P. E.; Fernandez, J. M. Reverse engineering of the giant muscle protein titin. *Nature* **2002**, *418*, 998–1002.

(25) Storm, C.; Pastore, J. J.; MacKintosh, F. C.; Lubensky, T. C.; Janmey, P. A. Nonlinear elasticity in biological gels. *Nature* **2005**, *435*, 191–194.

(26) Dobrynin, A. V.; Rubinstein, M. Theory of polyelectrolytes in solutions and at surfaces. *Prog. Polym. Sci.* **2005**, *30*, 1049–1118.

(27) Sheiko, S. S.; Sumerlin, B. S.; Matyjaszewski, K. Cylindrical molecular brushes: synthesis, characterization, and properties. *Prog. Polym. Sci.* **2008**, *33*, 759–785.

(28) Gradshteyn, I. S.; Ryzhik, I. M. *Table of Integrals, Series and Products*; Academic Press: New York, 1965.

(29) Plimpton, S. J. Fast parallel algorithms for short-range molecular dynamics. *J. Comput. Phys.* **1995**, *117*, 1–19. lammps.sandia.gov.

(30) Weiner, S. J.; Kollman, P.; Case, D. A.; Singh, U. C.; Ghio, C.; Alagona, G.; Profeta, S.; Weiner, P. A new force field for molecular mechanical simulation of nucleic acids and proteins. *J. Am. Chem. Soc.* **1984**, *106*, 765–784.